# UNIVERSITYOF BIRMINGHAM

# Synthesis and characterisation of a nucleotide based pro-drug formulated with a peptide into a nano-chemotherapy for colorectal cancer

Wilson, Jordan J.; Bennie, Lindsey; Eguaogie, Olga; Elkashif, Ahmed; Conlon, Patrick F.; Jena, Lynn; McErlean, Emma; Buckley, Niamh; Englert, Klaudia; Dunne, Nicholas J.; Tucker, James H.R.; Vyle, Joseph S.; McCarthy, Helen O.

Link to publication on Research at Birmingham portal

# Synthesis and characterisation of a nucleotide based pro-drug formulated with a peptide into a nano-chemotherapy for colorectal cancer

Jordan J. Wilson [a],[b], Lindsey Bennie [a], Olga Eguaogie [b], Ahmed Elkashif [a], Patrick F. Conlon [b], Lynn Jena [a], Emma McErlean [a], Niamh Buckley [a], Klaudia Englert [d], Nicholas J. Dunne [c], James H.R. Tucker [d], Joseph S. Vyle [b], Helen O. McCarthy [a],[e],*

[a] *School of Pharmacy, Queen's University Belfast, Medical Biological Centre, 97 Lisburn Road, Belfast BT9 7LB, UK*
[b] *School of Chemistry and Chemical Engineering, Queen's University Belfast, David Keir Building, Stranmillis Road, Belfast BT9 5AG, UK*
[c] *School of Mechanical and Manufacturing Engineering, Dublin City University, Centre for Medical Engineering Research, Dublin City University, Ireland*
[d] *School of Chemistry, University of Birmingham, Edgbaston, Birmingham B15 2TT, UK*
[e] *School of Chemical Sciences, Dublin City University, Collins Avenue, Dublin 9, Ireland*

ARTICLE INFO

ABSTRACT

Recent studies in colorectal cancer patients (CRC) have shown that increased resistance to thymidylate synthase (TS) inhibitors such as 5-fluorouracil (5-FU), reduce the efficacy of standard of care (SoC) treatment regimens. The nucleotide pool cleanser dUTPase is highly expressed in CRC and is an attractive target for potentiating anticancer activity of chemotherapy. The purpose of the current work was to investigate the activity of $P^1$, $P^4$-di (2′,5′-dideoxy-5′-selenouridinyl)-tetraphosphate ($P_4$-SedU$_2$), a selenium-modified symmetrically capped dinucleoside with prodrug capabilities that is specifically activated by dUTPase. Using mechanochemistry, $P_4$-SedU$_2$ and the corresponding selenothymidine analogue $P_4$-SeT$_2$ were prepared with a yield of 19% and 30% respectively. The phosphate functionality facilitated complexation with the amphipathic cell-penetrating peptide RALA to produce nanoparticles (NPs). These NPs were designed to deliver $P_4$-SedU$_2$ intracellularly and thereby maximise *in vivo* activity. The NPs demonstrated effective anti-cancer activity and selectivity in the HCT116 CRC cell line, a cell line that overexpresses dUTPase; compared to HT29 CRC cells and NCTC-929 fibroblast cells which have reduced levels of dUTPase expression. *In vivo* studies in BALB/c SCID mice revealed no significant toxicity with respect to weight or organ histology. Pharmacokinetic analysis of blood serum showed that RALA facilitates effective delivery and rapid internalisation into surrounding tissues with NPs eliciting lower plasma $C_{max}$ than the equivalent injection of free $P_4$-SedU$_2$, translating the *in vitro* findings. Tumour growth delay studies have demonstrated significant inhibition of growth dynamics with the tumour doubling time extended by >2weeks. These studies demonstrate the functionality and action of a new pro-drug nucleotide for CRC.

## 1. Introduction

Colorectal cancer (CRC) is the 4th most common cancer with the 2nd highest mortality rate in the UK at 11% and ~117 new daily diagnoses [1]. Current CRC standard of care (SoC) includes FOLFOX (Folinic acid, 5-fluorouracil and oxaliplatin) and FOLFIRI (Folinic acid, 5-fluorouracil and irinotecan) both of which contain 5-FU, a uracil homologue that functions to terminate DNA synthesis, causing cancer cell apoptosis [2,3]. Other SoC includes Capecitabine, and Trifluridine which are nucleoside analogues derived from pyrimidines that compete with endogenous nucleosides to yield antimetabolic activity [4–6].

Despite advancements in systemic therapy, SoC prolongs survival by 5-years [7]. This poor prognosis is attributed to numerous 5-FU resistance mechanisms; from innate evolution of drug transporters to acquired mutation of metabolic enzymes [8]. 5-FU is readily metabolised *in vivo,* leading to rapid clearance of the drug, necessitating prolonged treatment regimens and high doses of the therapeutic [9]. Additionally, 5-FU has poor membrane permeability and has been shown to be exported from cells *via* ATP-binding cassette (ABC) transporters, leading to resistance [10,11]. This may lead to reduced efficacy due to the inability of the drug to exert its intracellular therapeutic effects. With 90% of metastatic patients becoming resistant [12]. This necessitates the

---

need for new chemotherapies [13]. The enzyme, 2′-deoxyuridine 5′-triphosphate nucleotidohydrolase (dUTPase) is overexpressed in CRC compared to normal/healthy tissues by a factor of 2–5 [14,15]. dUTPase protects the cell by preventing genotoxic incorporation of 2′-deoxyuridine (dU) into DNA by converting the 2′-deoxyuridine 5′-triphosphate (dUTP) into the corresponding monophosphate, enabling cancer proliferation (Fig. 1) [16,17]. Furthermore, dUTPase can cause resistance to 5-FU by preventing bioaccumulation of the active 5-FU metabolite; 5-fluoro-2′-deoxyuridine 5′-triphosphate (5F-dUTP) [18].

Studies by Wilson [19] *et al* have demonstrated the function of wild-type and mutant p53 on the transcriptional modulation of dUTPase by the E2F-1 and Sp1 genes [20,21]. In HCT116 CRC cells, p53-mediated DNA-damage response caused by oxaliplatin treatment resulted in transcriptional downregulation of dUTPase, potentially sensitising cells to treatment with 5-FU [22]. Moreover, elevated dUTPase has been found in a range of CRC cancer cells including SW60 cells [23], which also display characteristic TS inhibition resistance attributed to the expression of dUTPase [24,25]. With 60% of CRC patients showing p53 dysregulation [26] the interplay between p53 and dUTPase expression, and the role in resistance, dUTPase is an attractive target for enhancing TS inhibitors yielding greater anticancer activity [27–30].

Kool [23] created a novel luminescence-based assay for the detection of dUTPase activity. This inspired the synthesis of a symmetric dinucleoside tetraphosphate designed to be specific to dUTPase and exploit its action. A symmetric tetraphosphate has the advantage of 'dual dosing', as the compound can be cleaved twice by dUTPase to yield two active moieties. However, phosphorylated compounds have limited bioavailability within cells and need to be delivered intracellularly for a therapeutic effect [31]. Intracellular barriers include crossing the cell membrane, escaping the endocytic cycle, efflux pumps, and non-specific phosphatases [32–34].

RALA is an amphipathic, fusogenic, cationic peptide that can penetrate through extra and intracellular barriers [35]. RALA is rich in arginine which confers positive charges at a physiological pH to encapsulate anionic cargoes, such as nucleic acids [36], and bisphosphonates [37] with efficient intracellular delivery of these cargos through fluorescent imaging. From these studies, it is clear that

RALA nanoparticles with a size of <200 nm and a positive charge >20 mv readily enter cells and escape endosomes, irrespective of the cargo [38,39]. RALA NPs have been utilised for injectable therapeutic and prophylactic vaccines as well as biomaterial devices such as microneedle arrays [40], thermo-responsive hydrogels [41], and electro-spun wound healing patches delivering a wide range of molecules [42]. Indeed, RALA/miR26a formulations remained stable over 28 days and up to 40 °C with respect to zeta potential and z-average [43]. Nanoparticles also remain intact and functional following exposure to heat inactivated and non-heat inactivated serum [43]. RALA delivers cargo *in vivo*, resulting in upregulated protein expression (for nucleic acid delivery) and therapeutic effects (for small molecule delivery) [38,44]. Nanoparticle-mediated delivery can be especially beneficial in oncology, where a discontinuous epithelium, coupled with leaky vasculature and reduced lymphatic drainage can lead to accumulation of the therapeutic at tumour sites. This is referred to as the enhanced permeability and retention (EPR) effect [45].

RALA NPs enable passage through cell membranes, are subsequently encased by an endosome and subjected to an environment of pH ≈ 4.5 by v-ATPase mediated proton influx [46,47]. Protonation of histidine instigates α-helicity of the peptide, aided by the glutamic acid and leucine residues. This concerted action causes endosomal membrane destabilisation, increases to the osmotic potential, and leads to release of the cargo from the endosome into the cytoplasm. Overall, the residues' combinatorial effects facilitate cargo in the cytosol and confer protection from degradation [36]. These effects have been demonstrated experimentally by performing transfections in the presence of chloroquine, a known endosomal disrupting agent, with no significant effect on transfection noted [38].

This study reports for the first time on the synthesis of a dinucleoside tetraphosphate prodrug that incorporates selenium which provides additional anticancer activity through a variety of proposed mechanisms including immune regulation, oxidative signaling and chemo preventive mechanisms [48–50]. The bioisostere modification changing the 5′ oxygen to selenium is postulated to not interfere with recognition by dUTPase [23,51,52], allowing liberation of an unstable monophosphate that spontaneously degrades to form an active selenol species, that
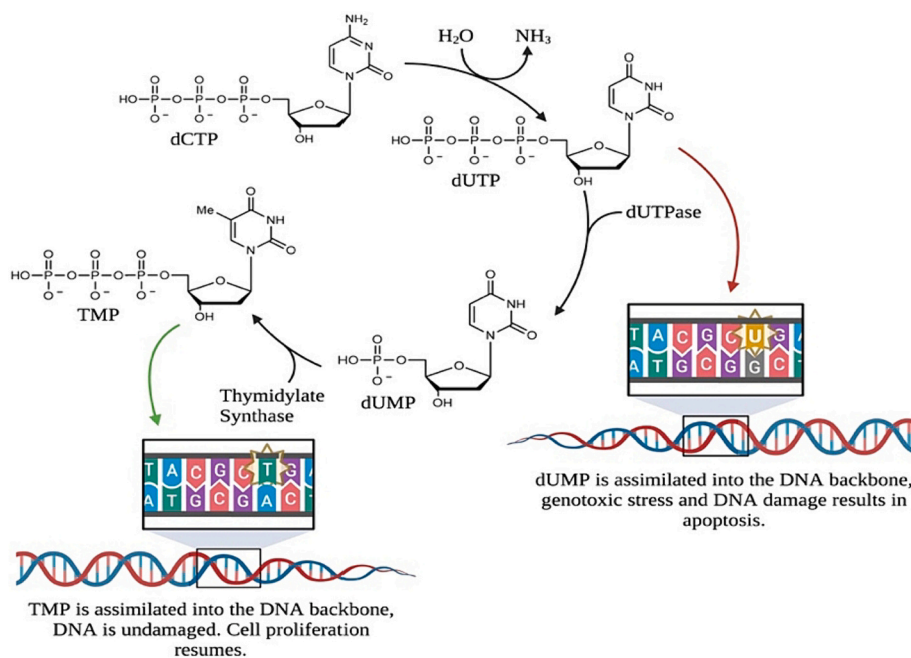


**Fig. 1.** Role of dUTPase. dUTP occurs naturally in the nucleotide pool by spontaneous deamination of dCTP. Assimilation of dUTP into the DNA chain yields genomic stresses and can result in apoptosis. The cell is protected by dUTPase by converting accumulated dUTP into dUMP which is sequentially converted to TMP by thymidylate synthase (TS).

exerts anticancer activity [48,50,53]. It is also hypothesised that complexation with RALA will result in improved bioavailability and efficacy as determined *via* i) the optimal mole ratio (MR) of RALA/$P_4$-SedU$_2$ in terms of physiochemical characteristics, cellular uptake, functionality and specificity for dUTPase; ii) the pharmacokinetic profile of RALA/$P_4$-SedU$_2$ NPs compared to $P_4$-SedU$_2$ alone; and iii) the *in vivo* safety profile, dosing profile and anti-tumour efficacy.

## 2. Materials & methods

Information regarding total synthesis of $P_4$-SedU$_2$ and $P_4$-SeT$_2$ including NMR, MS, HPLC spectra and methodologies, detailed nanoparticle formulation rationale, lyophilisation recipe, RT-qPCR primers and full *in vivo* protocols, can be found in the supplementary information. RALA (NH$_2$-WEARLARLALRALARHLARALARALRACEA-CO$_2$H) (RFM: 3327.98 g mol-1) was synthesised by solid state FMOC Chemistry and provided in the acetate salt form at ≥95% purity as a lyophilised powder (Biomatik, USA) and stored at −20 °C. RALA when used is reconstituted to 1.0 μg/μL (determined using Nano-Drop 2000C spectrophotometer using pre-set protein A280 setting (Thermoscientific, USA) for use to formulate nanoparticles. For lyophilisation protocols, trehalose (Pfanstiehl, USA, No. T104–4) was dissolved in Ultrapure DNase / RNase free water (Invitrogen, UK) at 20% *w/v* was used as the cryoprotectant and lyoprotectant.

### 2.1. Formulation and characterisation of RALA nanoparticles

Nanoparticles (NP) were assembled by pipetting the required volume of $P_4$-SedU$_2$, or $P_4$-SeT$_2$ at 0.5 mg/mL to achieve 1 nmol in solution followed by an aliquot of H$_2$O and finally varying volumes of RALA at 1.0 mg/mL (to give stoichiometric ratios of 1:1 to 10:1 peptide/cargo) in a final volume of 50 μL. The solution was incubated at ambient temperature (~21 °C) for ~30 min before characterisation. Formulated NPs were characterised using a Malvern Nano-ZS Zetasizer (Malvern Instruments, UK). 50 μL of NP sample was placed in a 2 mL disposable microcuvette and was used to characterise the NP size using the *Z*-average parameter measured in diameter nm (d.nm) by means of dynamic light scattering (DLS). The 50 μL NP sample was diluted to 1 mL and transferred to a 1 mL disposable folded-capillary zeta-cell cuvette and was used to characterise the NP charge potential using the zeta potential parameter and measured in mV by means of laser doppler velocimetry (LDV). Both analyses were carried out at 20 °C. For transmission electron microscopy (TEM), 2:1 mol ratio of RALA/$P_4$-SedU$_2$ NPs were produced, lyophilised, and loaded onto carbon reinforced 400 mesh copper grids (TAAB laboratories, UK) for 15 min before overnight drying, subsequent staining with Uranyless EM stain (EMS, USA) for 5 min at RT and dried overnight. The samples were imaged using a JEOL-JEM 1400 Plus TEM (JEOL, USA) at a 80 kV accelerating voltage.

### 2.2. Cell culture & maintenance

HCT116 CRC and HT29 CRC cell lines (ATCC, USA) were maintained in McCoy's 5 A serum; modified with L-Glutamine (Invitrogen, UK) and supplemented with 10% FCS (Invitrogen, UK). NCTC-929 fibroblast cell lines were maintained in Dulbecco's Modified Eagles Medium (Invitrogen, UK) and supplemented with 10% foetal calf serum (Invitrogen, UK). All cells were cultivated in T75 flasks and grown as monolayers in a humidified incubator at 37 °C and 5% CO$_2$ conditions. At *ca.* 80% confluency, cells are passaged using 10% *v*/v trypsin in phosphate buffered saline (PBS) to detach the monolayer and then neutralised with a corresponding volume of culture media, followed by centrifugation and removal of the supernatant. The cell pellet was resuspended in culture media and re-seeded in flasks to maintain exponential growth. Cell genotypes are authenticated by short-tandem repeat (STR) profiling by the suppliers and routine monthly testing ensures no *mycoplasma* contamination is present during *in vitro* research.

### 2.3. Cell viability assay

Cell viability was assessed using alamarBlue™ (Invitrogen, UK). HCT116 & HT29 CRC cell lines were seeded onto 96-well plates at $0.5 \times 10^4$ and $1.5 \times 10^4$ cells per well respectively and incubated overnight at 37 °C and 5% CO$_2$ to adhere to the well surface to form a monolayer. Culture media was replaced with OptiMEM (Invitrogen, UK) 2 h prior to treatments with lyophilised RALA NPs to achieve final exposure concentrations from $1 \times 10^{-4}$– $1 \times 10^{-9}$ M respectively. Drug-only controls were also performed to the equivalent concentrations. Cells were incubated for 6 h with the treatments and then replaced with culture media and incubated for 1–3 days at 37 °C and 5% CO$_2$ and cell viability was assessed using alamarBlue™ (non-toxic cellular reduction of resazurin to resorufin) (Invitrogen, UK) at 24 h intervals. AlamarBlue™ was added to a final concentration in culture media of 10% and incubated (avoiding light) for 2–4 h, after which 50 μL of the 10% alamarBlue™ media was transferred to black 96-well plates and recorded using fluorescence with excitation 530 nm and emission of 590 nm using a FLUOstar Omega microplate reader with MARS data analysis software (BMG Labtech, UK). Cell viability data was normalised from the untreated cells as 100% to the null-cell blank as 0% and EC$_{50}$ was calculated as half-maximal response using GraphPad Prism v10.0.3 (GraphPad Software, USA) and using eq. Y = 100/(1 + 10ˆ((LogEC50-X)*HillSlope)).

### 2.4. Clonogenic survival assay

HCT116 and HT29 CRC cell lines were plated onto 6-well plates at a density of $1.5 \times 10^5$ cells per well and incubated overnight at 37 °C and 5% CO$_2$ to adhere to the well surface to form a monolayer. Culture media was replaced with OptiMEM (Invitrogen, UK) 2 h before treatments. Cells were then treated for 6 h with uncomplexed dinucleoside tetraphosphate and NPs at a concentration respective to the cell line EC$_{50}$, with a trehalose negative control at the equivalent percentage concentration as the reconstituted lyophilised NPs and untreated well control. Following 6 h treatments, cells were washed with PBS and detached using 1× trypsin in PBS. Culture media is added to neutralise the trypsin and cells are centrifuged at 1500 rpm for 5 min. The cell pellet is resuspended in culture media and vortexed gently to homogeneity and counted using the Beckman-Coulter counter (Beckman-Coulter, IRE). Each cell experiment is plated at cell densities of 250, 500, 750 and 1000 cells with 3 replicates per density, cells are placed back in an incubator at 37 °C and 5% CO$_2$ for 14 days. Culture media was decanted, and colonies fixed with 0.4% crystal violet in 70% MeOH for 15 min, decanted and washed with H$_2$O and dried for 24–48 h before manual colony counting. Plating efficiencies and surviving fractions were calculated as per Nature Protocol [54].

### 2.5. Spheroid culture

HCT116 CRC cell lines were seeded onto a 96-round-bottom well plates at $0.5 \times 10^4$ cells per well and incubated overnight at 37 °C and 5% CO$_2$. Spheres were allowed to grow for one week and monitored to establish spheroid growth profiles. After a week, culture media was carefully replaced with OptiMEM (Invitrogen, UK) 2 h before treatments with lyophilised 2:1 RALA/$P_4$-SedU$_2$ NPs to achieve final exposure concentrations from $1 \times 10^{-5}$– $1 \times 10^{-9}$ M respectively. $P_4$-SedU$_2$ only controls were also added to the equivalent concentrations. Cells were incubated for 6 h with the treatments and then replaced with culture media and incubated for 1 day at 37 °C and 5% CO$_2$. Spheroid volume was assessed using the Cell3iMager X neo (SCREEN, JPN) cell imager and software to calculate approximate spheroid volumes.

### 2.6. mRNA extraction

HCT116 and HT29 cells were plated onto 6-well plates with appropriate culture media and grown until ~100% confluent. Culture media

was discarded and 1 mL TRIzol reagent (Invitrogen, UK) was added to each well and scraped to completely lyse cells and dissociate nucleic acid content. TRIzol / cell lysate mixture was transferred into 1.5 mL tubes, 0.2 mL of $CHCl_3$ was added, and vortexed for 5 s, and then incubated for 2 min. The mixture was centrifuged for 15 mins at 12,000 g at 4 °C and the supernatant was transferred into new 1.5 mL tubes. 0.5 mL of isopropanol was added to the extracted nucleic acid mixture, vortexed for 5 s and incubated overnight at 4 °C to facilitate complete mRNA precipitation and then centrifuged for 15 min at 12,000 g at 4 °C to form a mRNA pellet. The mRNA pellet was resuspended in 1 mL of EtOH and vortexed for 5 s and centrifuged for 5 min at 7500 *g* at 4 °C. The supernatant was discarded, and the mRNA pellet was partially dried before resuspension in $ddH_2O$ where yield and quality was determined using a Nano-Drop 2000C spectrophotometer (Thermoscientific, USA). An A260/A280 ratio ~ 1.8–2.0 and A260/A230 ratios ~2.0–2.2 are considered pure.

## 2.7. cDNA synthesis

HCT116 and HT29 mRNA samples were used to produce the corresponding cDNA using Transcriptor First Strand cDNA Synthesis kit (Roche, SUI). mRNA was analysed and diluted with $ddH_2O$ to obtain a working concentration of 0.1 µg/µL (10 µL total volume required per reaction well). Each reaction well requires 1 µL of Anchored-Oligo Primer and 2 µL of Random Hexamer Primer (this is performed in duplicate to provide samples for reverse transcriptase (RT) negative reactions). The final reaction volume is 13 µL and the sample is placed into a thermocycler at 65 °C for 10 min. After denaturation, each reaction well has 4 µL of 5× Reaction Buffer, 0.5 µL RNase Inhibitor, 2 µL DNTP mix and 0.5 µL RTase (equivalent volume of $ddH_2O$ is added in place for the RT negative reaction wells). The total reaction volume is 20 µL. Reaction wells were placed into the thermocycler, at 25 °C for 10 min – 55 °C for 30 min – 85 °C for 5 min and then stored on ice. cDNA was stored at −20 °C until further use in PCR.

## 2.8. RT-qPCR

RT-qPCR was performed using a LightCycler® 480 SYBR Green I Master (Roche, SUI). Theoretically, 1 µg of RNA in 20 µL yields 50 ng $µL^{-1}$ of cDNA. The cDNA solution is diluted to 5 ng $µL^{-1}$ for experimental use. To each reaction well, 5 µL of SYBR, 0.5 µL of forward and reverse primers (5 µM), and 4 µL of cDNA is added. The SYBR and primers are prepared separately as a master mix by adding the total volume required of both SYBR and the primers together before adding 6 µL of the master mix to the cDNA reaction wells. The PCR is run on a LightCycler 480 and the annealing step must be set to 2–3 °C lower than the lowest Tm of the primers used in the experiment.

## 2.9. Animals

BALB/c SCID mice were purchased from Charles River Laboratory (USA) and housed in an open pathogen controlled clean zone at 21 °C at 50% relative humidity with a supply of food and water *ad libitum*. All protocols and procedures conform to the UK scientific act of 1986 and are covered by the Department of Health, Social Services and Public Safety, Project License 2903 and Personal License 2128.

## 2.10. Statistical analysis

Statistical analyses were performed using GraphPad Prism v10.0.3 (GraphPad Software, USA). Statistically significant differences were calculated using a one-way ANOVA, two-way ANOVA, or unpaired *t*-test, preferring parametric analysis only if normality and lognormality tests pass (alpha = 0.05), otherwise nonparametric tests are used. *p*-value of $\leq 0.05$ considered significant, (*) $p \leq 0.05$, (**) $p \leq 0.01$, (***) $p \leq 0.001$.

## 3. Results & discussion

### 3.1. Synthesis and characterisation of selenium-modified dinucleoside tetraphosphate analogues $P_4$-SedU$_2$ (4a) and $P_4$-SeT$_2$ (4b)

To introduce the selenium at the 5′-position of 2′-deoxyuridine (dU) or thymidine (T), b Selenocyanate-mediated displacement of a 5′-tosylate in refluxing anhydrous acetonitrile gave the corresponding nucleoside 5′-selenocyanates 1a or 1b (Scheme 1). Phosphate coupling using acid-promoted P—N bond activation under Khorana-type solution-phase conditions [55] is complicated by the sensitivity of the P—Se moiety in precursor phosphoroselenolate monoesters towards cleavage in the presence of aqueous acid [56]. In contrast, the corresponding persilylated monoesters such as the selenonucleoside derivatives 2a and 2b are relatively stable when stored under anhydrous conditions and can be readily accessed in near quantitative yields (by $^{31}$P NMR) following reaction of the corresponding selenocyanates (1a and 1b) with tris (trimethylsilylphosphite).

Our group has recently exploited mechanochemistry to provide access to dinucleoside pyrophosphate analogues containing P-Se-C$^{5'}$ linkages [57] *via* intermediates such as 2b following *in situ* hydrolytic desilylation and coupling with AMP-morpholidate [58,59] in a vibration ball mill (VBM). More efficient phosphate coupling in a VBM was described subsequently using reactive NMP-imidazolide substrates generated *in situ* to access di-, tri- and tetraphosphate-linked dimers. [60,61] Following these latter reports, we attempted *in situ* hydrolytic desilylation and coupling of 2a or 2b with half an equivalent of the pyrophosphate bis-imidazolide coupling partner 3 [62] under mechanochemical activation.

Crude reaction mixtures were analysed by $^{31}$P NMR following VBM for 90 min. Under optimised conditions (1.5 equivalents MgCl$_2$.6H$_2$O and 13 equivalents H$_2$O) complete consumption of 3 ($\delta_P$ -20.94) was observed. The reaction mixtures were extracted from the vessel in buffer (pH 7.4) and the filtered suspension subjected to ion-pair, reversed-phase HPLC purification. Pure 5′,5″-linked dinucleoside tetraphosphate analogues were isolated following desalting with a volatile buffer, co-evaporation with water and finally ion exchange chromatography. The sodium salts of $P_4$-SedU$_2$ (4a) and $P_4$-SeT$_2$ (4b) were fully characterised by multinuclear NMR (*e.g.*, $^{31}$P and $^{77}$Se - Scheme 1) and mass spectrometry.

### 3.2. Formulation and characterisation of RALA NPs

RALA NPs were synthesised using mole ratios (RALA:$P_4$-SedU$_2$ and RALA: $P_4$-SeT$_2$) from 1:1 to 10:1 and then lyophilised to overcome cold-chain storage limitations with trehalose as the lyoprotectant [63]. Previous work on the RALA peptide by Massey *et al* [64] revealed the capacity of RALA to complex phosphorous containing small molecules. Those formulations were based on a mass-mass ratio of cargo and RALA. The use of a mole-mole relationship was employed in this study as it better describes the quantity of RALA molecules necessary for successful encapsulation of a single molecule of cargo. Using mole ratios, which can be compared across molecules, $P_4$-SedU$_2$ and $P_4$-SeT$_2$ successfully form NPs upon mixing with RALA (Fig. 3), apart from mole ratio 1:1 with dTSep4SedT (shown in supplementary information). Ideal NPs were produced with a 2:1 mol ratio for RALA: $P_4$-SedU$_2$ NPs and 5:1 mol ratio for RALA: $P_4$-SeT$_2$ NPs. The NPs had a size <150 nm diameter (size and morphology of particles is confirmed with transmission electron microscopy (TEM)), a charge >10 mV and a relatively homogenous population with a PdI of <0.4 (Fig. 2); characteristics that are ideal for cellular uptake and stability [65,66]. $P_4$-SeT$_2$ NPs are larger, less homogenous and require more RALA to successfully form NPs compared to $P_4$-SedU$_2$. This may be attributed to steric hindrance by the C5 methyl, reducing electrostatic interactions between with RALA [67]. Lyophilisation of the 2:1 mol ratio RALA: $P_4$-SedU$_2$ NPs improved the PdI to <0.2, and had no significant impact on the distribution spectra of 5:1
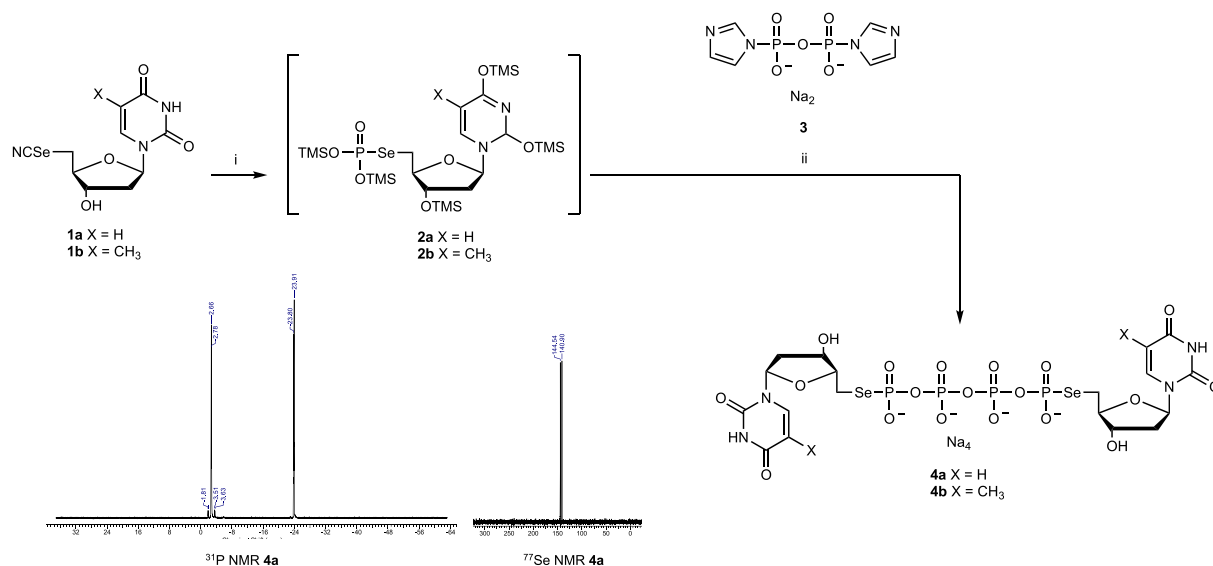
**Scheme 1.** Synthesis of selenium modified dinucleoside tetraphosphates. i) BSA (13.1 eq.) TMSO$_3$P (1.1 eq.), CHCl$_3$, rt, 12 h (2a, 2b > 99%, 4b > 99% - by $^{31}$P NMR). ii) 3 (0.5 eq.), MgCl$_2$.6H$_2$O (1.5 eq.), H$_2$O (13.0 eq.), 30 Hz, 1.5 h (4a 19%, 4b 30%).



| A | Characteristics | | |
|---|---|---|---|
| **NP and mole ratio** | Z-Average (nm) | Zeta Potential | PdI |
| **2:1 RALA / P$_4$ - SedU$_2$** | 103.3 nm | 18.1 mV | 0.247 |
| **5:1 RALA / P$_4$ - SeT$_2$** | 138.4 nm | 22.6 mV | 0.391 |
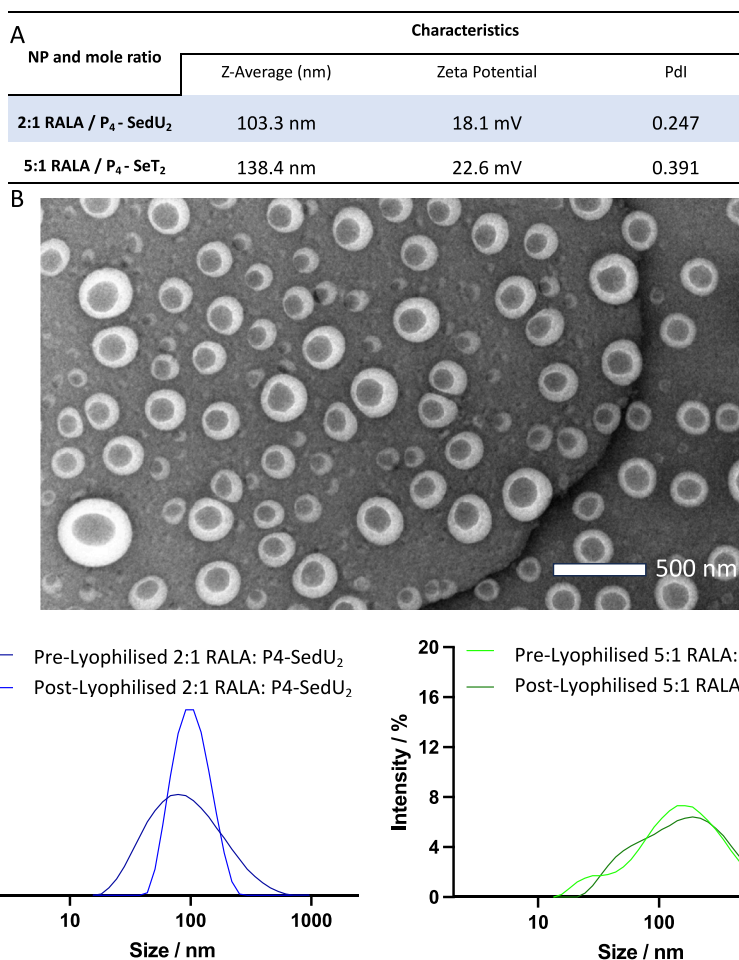
**Fig. 2.** Nanoparticle formulation and characterisation of lyophilised RALA NPs. A) Size, charge, and Polydispersity characteristics of lyophilised 2:1 RALA/P$_4$-SedU$_2$ NPs and lyophilised 5:1 RALA/ P$_4$-SeT$_2$ NPs. B) Transmission Electron Microscopic image of lyophilised 2:1 RALA/P$_4$-SedU$_2$ NPs (Scale bar = 500 nm). C) DLS spectrographs of pre and post lyophilised 2:1 RALA/ P$_4$-SedU$_2$ NPs, and pre and post lyophilised 5:1 RALA/ P$_4$-SeT$_2$ NPs.
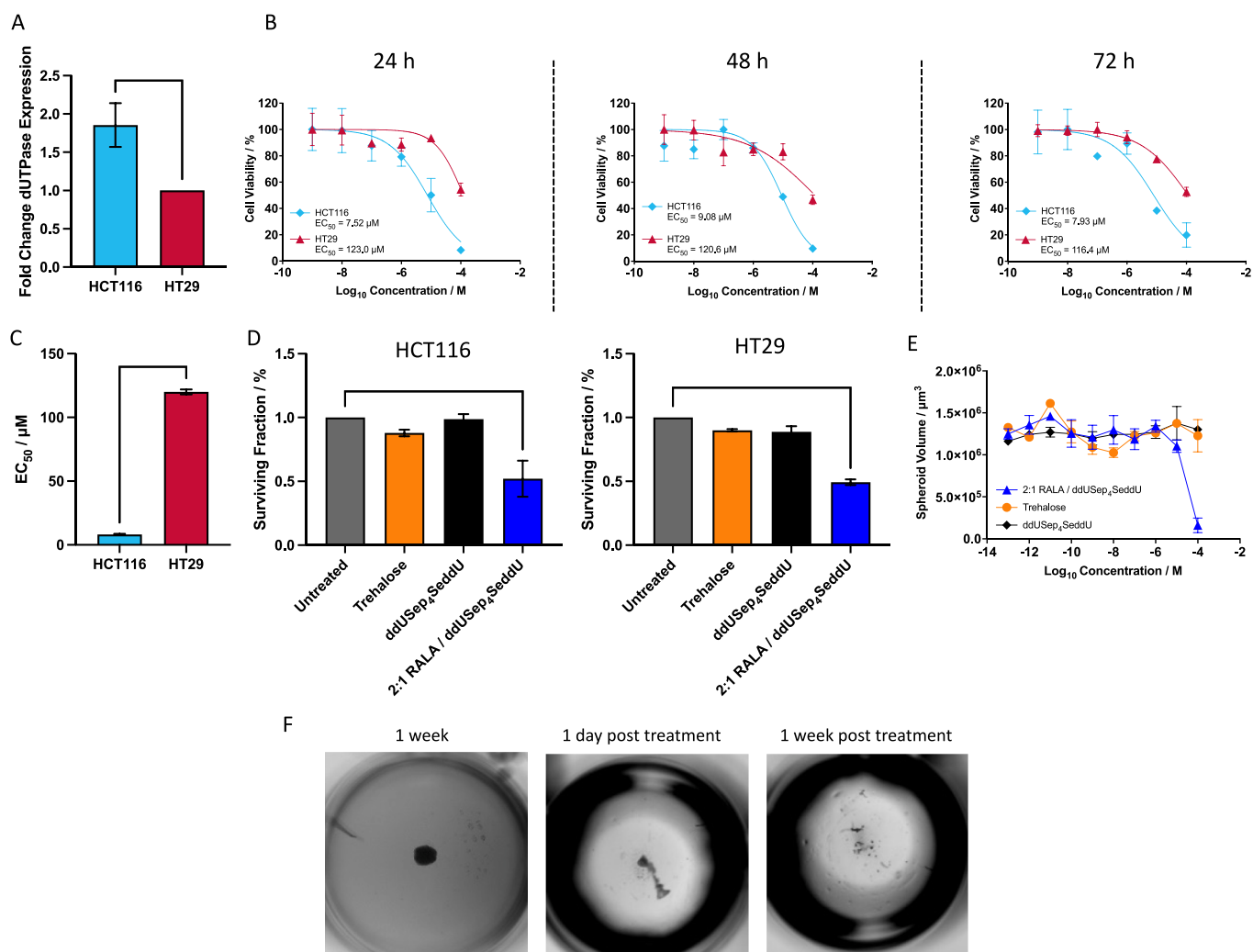
**Fig. 3.** dUTPase activity and anticancer efficacy in HCT116 and HT29 cells. A) Fold change difference in dUTPase expression by RT-qPCR in HCT116 cells compared to HT29 cells. Results are normalised to dUTPase expression in HT29 cells. B) Cell viability of HCT116 (light blue) and HT29 (red) cells with lyophilised 2:1 RALA/P$_4$-SedU$_2$ NPs over 3 days at 24 h intervals. C) Difference in average EC$_{50}$ value over 3 days between HCT116 and HT29 cells when treated with 2:1 RALA/P$_4$-SedU$_2$. D) Clonogenic survival assays on HCT116 and HT29 cells with treatments of trehalose, P$_4$-SedU$_2$ only and 2:1 RALA/P$_4$-SedU$_2$ at the corresponding observed EC$_{50}$ values of 2:1 RALA/P$_4$-SedU2 treatments. E) Spheroid volume of HCT116 cells after 7 days after treatment with trehalose, P$_4$-SedU$_2$ only and 2:1 RALA/P$_4$-SedU$_2$. F) Photographs of spheroid of HCT116 cells, 1 week after plating, 1 and 7 days after treatment with 2:1 RALA/P$_4$-SedU2.

mol ratio RALA: P$_4$-SeT$_2$ NPs (Fig. 3). These findings prove that the formulated nanoparticles can be lyophilised, allowing ease of storage without compromising physicochemical characteristics.

### 3.3. Potentiating an anticancer response in vitro

The anti-cancer effects of the 2:1 RALA/P$_4$-SedU$_2$ were interrogated *via* cell viability, clonogenic assay, and 3D culture experiments on the HCT116 and HT29 cell lines; two colorectal cancer cell lines with reported high and low dUTPase expressions respectively [68–70]. This was confirmed by RT-qPCR revealing dUTPase expression is $1.9\times$ fold higher in HCT116 cells compared to HT29 (Fig. 3 A). This was reflected in the viability assay where 2:1 RALA/P$_4$-SedU$_2$ (Fig. 3 B and C) had significantly lower anticancer activity ($p \leq 0.0001$) in HT29 cells with an EC$_{50}$ of >115 μM compared to >7.5 μM in the HCT116 cell across all time points. Despite a mere 1.9-fold difference in dUTPase there was a > 15 fold enhancement in activity which is indicative of significant potentiation. These results indicate that higher dUTPase levels present in HCT116 cells facilitate greater release of the active metabolite, leading to greater cytotoxicity.

Clonogenic survival studies (Fig. 3 D) were performed to assess

impacts on tumourigenicity, using corresponding 3-day EC$_{50}$ dose of the 2:1 RALA/P$_4$-SedU$_2$ NP treatments of 8.2 μM on HCT116 and 360 μM on HT29 which resulted in 50% reduction in colony formation. Trehalose was also included as a control as carbohydrate can potentiate an independent m-TOR pathway to induce autophagy [71,72] thus promoting proliferative effects in HCT116 cells. However, the addition of trehalose controls had no significant effect on proliferation on either cell line. The 2:1 RALA/P$_4$-SedU$_2$ NP treatments outperformed free P$_4$-SedU$_2$, indicating that efficient intracellular trafficking of the drug is required to exert a cytotoxic effect.

The 3D culture yielded a reduction in anti-cancer activity when treated with an EC$_{50}$ of 22.33 μM in HCT116 spheroids (Fig. 3 E), which could be attributed to the formation of an extra cellular matrix (ECM) from increased cell-cell interactions. The ECM can act as a barrier to drug delivery by trapping NPs within the collagen rich matrix. Additionally, penetration into the inner core is diminished in spheroid cultures. Although spheroids provide a pseudo-tumour environment, with ECM, hypoxia and angiogenic factors present, fundamentally they do not have the tortuous vasculature to support the transport of nanoparticles [73,74]. Other studies have found similar results with the EC$_{50}$ increasing between 2D and 3D cultures depending on; the 3D scaffold

used, cell type, particle size, and the relative tissue densities within the 3D culture [75–77].

It was observed with the highest dose of 100 μM, that the cellular structures were abolished after 7 days, (Fig. 3 F) leaving scattered fragments indicating internal stresses on the cellular architecture. Selenol species' are highly reactive and can destabilise disulfide bridges [78–80], that are found in lysosomal proteins, lumen of the RER, mitochondrial intermembrane space, and collagen III [81]. In addition, the potential to trigger nucleocytoplasmic coagulation, a terminal cascade triggered by cellular-injury causes proteolytic destruction of the cellular contents into macromolecular aggregates. This then results in apoptosis to prevent uptake of misfolded proteins [82]. It has been shown in nucleic acid and small molecule delivery studies that problems typically arise due to the extra cellular effects in 3D models that are not found in 2D cultures. However, efficacy in a 3D model does provide confidence that a therapeutic effect would be observed *in vivo* [83–85]. Herein, the 3D model results indicate that the potency of the RALA/$P_4$-SedU$_2$ NPs should be retained *in vivo*.

### 3.4. Specificity of dUTPase in vitro

The 5:1 RALA/$P_4$-SeT$_2$ NPs were used on the HCT116 cell line to test the specificity of dUTPase to the uracil motif on the drug molecules. Work by Vertessy [52,86] used computational modelling to show that the dUTPase active site is robust enough to differentiate dUTP and dTTP and prevent mis binding. These findings were confirmed *in vitro* by Kool [23]. 5:1 RALA/$P_4$-SeT$_2$ NPs do not induce any anticancer activity (Fig. 4) supporting the specificity of $P_4$-SedU$_2$.

Experimental data provides evidence to support the hypothesis that the dUTPase active site is specific to uridine, where scission between the α and β phosphates occurs to liberate a monophosphate and triphosphate species, to release the anti-cancer potential of the selenols (Fig. 4). Zeng observed a 2.2-fold increase in cellular apoptosis with 5 μM treatments with methylselenol on HCT116 cells. Zeng also reported that selenol species interrupt protein-thiol moieties on redox responsive signaling and transcription factors (E2F) [19] ultimately leading to G$_1$ arrest, and diminution of MMP-2 and VEGF [49,87–89]. Further investigations into the downregulation of MMP-2 and VEGF would need to be performed to build a better understanding of the downstream mechanisms with $P_4$-SedU$_2$. Furthermore, the uncomplexed materials (Fig. 3 D & Fig. 4) also do not elicit anti-cancer activity, revealing the necessity of RALA, as negatively charged molecules are unable to penetrate the cell [90,91].

The evidence presented indicates that patients could be stratified based on dUTPase expression prior to treatment with RALA/$P_4$-SedU$_2$, and those with the highest dUTPase expression could be predicted to have an improved response as this would be the first dUTPase targeted chemotherapy. This personalised approach to treatment is advantageous compared to other chemotherapies such as cisplatin which are administered indiscriminately and target all genomic DNA in replicating cells [92–96].

### 3.5. Establishing safety and pharmacokinetics

To investigate potential anticancer effects *in vivo* on tumour models, safety studies were initially performed to establish potential cytotoxicity. Firstly, *in vitro* treatments with 2:1 RALA/$P_4$-SedU$_2$ NPs were
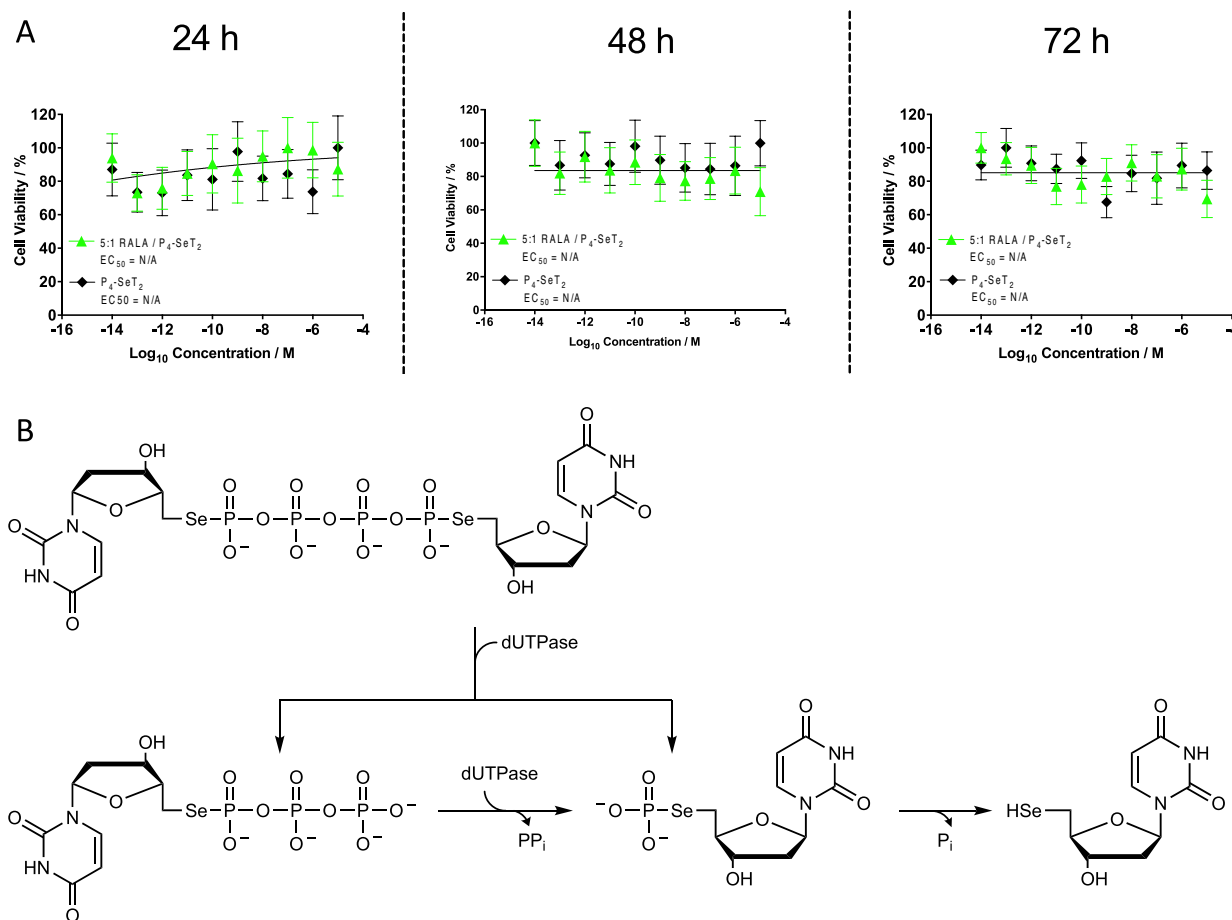


**Fig. 4.** Determination of 5:1 $P_4$-SeT$_2$ NPs EC$_{50}$ on dUTPase positive HCT116 cells. A) Cell viability studies on HCT116 cells over 72 h following treatment with uncomplexed $P_4$-SeT$_2$ or 5:1 RALA/$P_4$-SeT$_2$ NPs. B) Theoretical mechanism of action of dUTPase activity on the $P_4$-SedU$_2$. Scission between the α and β phosphates may liberate an unstable monophosphate species which dephosphorylates the corresponding selenol, which could cause anticancer activity.
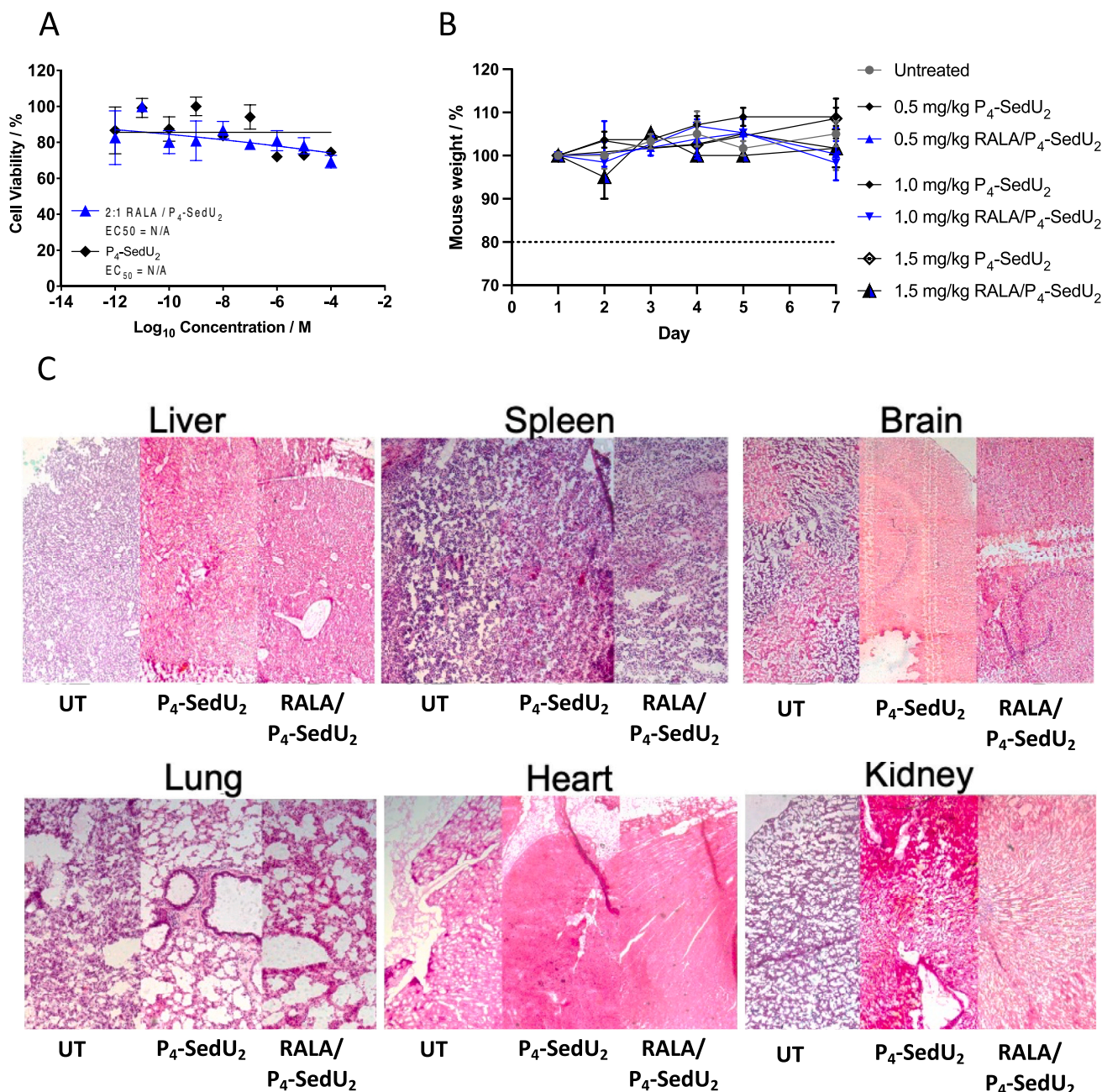
**Fig. 5.** Investigation into the safety profile of $P_4$-SedU$_2$ and RALA NPs. A) Cell viability assay on NCTC-929 cells with 2:1 RALA/$P_4$-SedU$_2$ and $P_4$-SedU$_2$ only after 24 h. B) Mouse weight measurements of MTD study. Untreated control, 0.5–1.5 mg/kg doses of $P_4$-SedU$_2$ only and 2:1 RALA/$P_4$-SedU$_2$, NPs. C) Histology slides of H&E-stained mouse organ sections from MTD study, $10\times$ magnification. Each slide represents the corresponding organ and directly comparing treatments. UT = untreated, $P_4$-SedU$_2$ = 1.5 mg/kg 2:1 RALA/$P_4$-SedU$_2$, and RALA/$P_4$-SedU$_2$ = 1.5 mg/kg $P_4$-SedU$_2$ only.

performed on the NCTC-929 murine fibroblast cell line to investigate the impacts on non-neoplastic tissues (Fig. 5 A). This revealed a non-cytotoxic response, as there is no significant impact on cell survival with the concentration used for an effective treatment on HCT116 cells, since a cell viability <70% is considered cytotoxic [97].

A minimal effective dose (MED) study was performed on BALB/c SCID mice; using doses of 0.5 mg/kg, 1.0 mg/kg and 1.5 mg/kg of either 2:1 RALA/$P_4$-SedU$_2$ NPs or $P_4$-SedU$_2$ only (Fig. 5 B). Results revealed no significant weight change throughout the week of experiment, and no mice weights dropping below the 20% weight-loss threshold. In addition, health checks 1 h, 3 h, 5 h, and 24 h post treatment showed no signs of distress or negative behavioural characteristics. This was supported by histology of vital organs (Fig. 5 C). Evaluations of the organ sections

of untreated and treated mice with 1.5 mg/kg (0.5 & 1.0 mg/kg not shown) of both $P_4$-SedU$_2$ only and 2:1 RALA/$P_4$-SedU$_2$ NPs displayed no signs of necrotic tissue within the gross structures.

Pharmacokinetic (PK) analysis was performed to investigate differences between $P_4$-SedU$_2$ only and 2:1 RALA/$P_4$-SedU$_2$ NPs with respect to drug exposure, bioavailability, clearance, metabolism, and excretion [98,99]. Mice were treated with 1.5 mg/kg $P_4$-SedU$_2$ only and 2:1 RALA/$P_4$-SedU$_2$ NPs, and sampled at 0.25 h, 0.5 h, 1 h, 5 h post treatment (Fig. 6). The $P_4$-SedU$_2$ only treatment is highly present in the blood plasma compared to the 2:1 RALA/$P_4$-SedU$_2$ NP treatment, with a $C_{max}$ of 21.174 mg/L compared to 2.394 mg/L respectively. The AUC is 76.74 mg*h/L for the $P_4$-SedU$_2$ only, which was $4.4\times$ higher than then 2:1 RALA/$P_4$-SedU$_2$ NPs treatment. Both $T_{max}$ values were the same for both
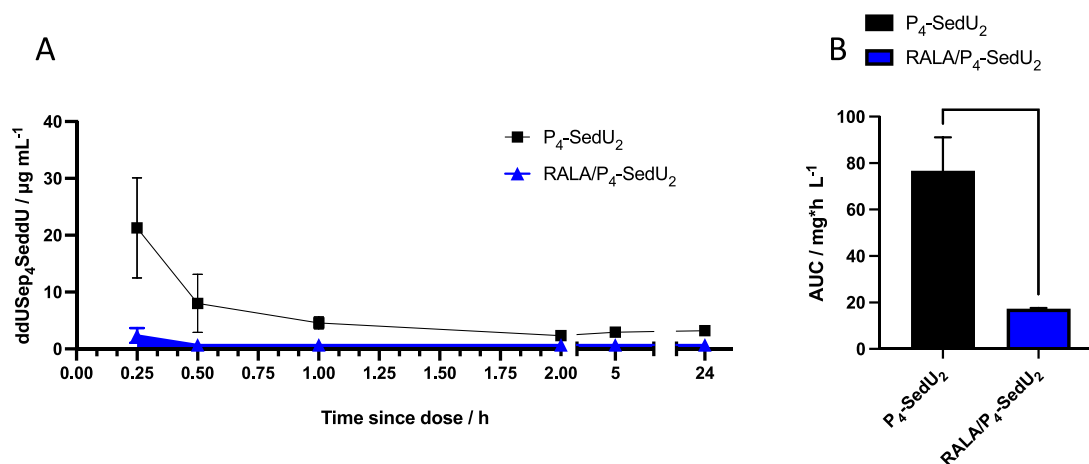
**Fig. 6.** Pharmacokinetic Data of 1.5 mg/kg $P_4$-SedU$_2$ and RALA/$P_4$-SedU$_2$ NP treatments. A) Recovered $P_4$-SedU$_2$ (μg/mL) over time (from 0.25 to 24 h, $N = 3$ for each time point) Area under curve (AUC) highlighted. Concentration of $P_4$-SedU$_2$ was extrapolated from standard curve of peak area ($R^2 = 0.9922$) in mg/L. B) AUC plot and unpaired *t*-test statistics reveal significance ($p \leq 0.05$) between the two treatments, AUC represents total exposure to analyte $N = 3$.

**Table 1**

$P_K$ parameters extrapolated from PK profile, Area Under the Curve (AUC), Maximum concentration ($C_{max}$), Time to maximum concentration ($T_{max}$) and putative half-life ($T_{1/2}$).

| | AUC$_{[0-24\ h]}$ [mg*h/L] | C$_{max}$ [mg/L] | T$_{max}$ [min] | T$_{1/2}$ [min] |
|---|---|---|---|---|
| $P_4$-SedU$_2$ | 76.74 | 21.17 | 15 | 23.3 |
| 2:1 RALA/$P_4$-SedU$_2$ NPs | 17.36 | 2.39 | 15 | 17.1 |

treatments, showing highest concentrations with the first sample point. $P_4$-SedU$_2$ had a longer half-life compared to the 2:1 RALA/$P_4$-SedU$_2$ NPs treatment, with a $T_{1/2}$ value of 23.3 min compared to 17.1 min (Table 1).

$P_K$ studies of prodrugs typically investigate the concentration of the active metabolite [100], however in this study only the parent molecule was observed. The putative metabolite ddUSeH was not readily available to build the standard curve by HPLC. The metabolite could not be extracted from an enzyme digest study, as during the synthesis of $P_4$-SedU$_2$. the ddUSeH species spontaneously forms the corresponding diselenide that would readily precipitate out of solution, causing issues with HPLC analysis. Such studies will be investigated in future to confirm biodistribution of the active metabolite. Herein, the results above represent the inverse effect. The AUC represents total exposure in plasma, and results indicate that the 2:1 RALA/$P_4$-SedU$_2$ NPs treatment was being delivered and retained within the exposed tissues/cells as it has a much lower concentration in plasma compared to $P_4$-SedU$_2$ which is unable to penetrate the intracellular environment and thereby is retained within the plasma and eliminated. Additionally, the rate of uptake of 2:1 RALA/$P_4$-SedU$_2$ NPs into tissues indicates a rapid process of cellular uptake as the $C_{max}$ value was 8.8-fold less than the $P_4$-SedU$_2$ treatment, this effect is reflected with the shorter half-life time of 17.1 mins with the 2:1 RALA/$P_4$-SedU$_2$ NPs treatment.

These results correlate with other $P_K$ analyses of prodrugs where DB289 (an anti-fungal prodrug) by Trendler exhibited similar $P_K$ characteristics to the parent compound with a rapid $T_{max}$ values followed by rapid elimination in Sprague-Dawley albino rats [98]. Furthermore, reduction in AUC is observed with PEGylated NPs of 5-FU and gemcitabine, while both treatments significantly improving anti-tumour efficacy in CRC and breast cancer xenograft studies respectively [101–103]. The results in the present study, indicate that RALA rapidly delivers of $P_4$-SedU$_2$ into surrounding tissues thus preventing rapid elimination.

### 3.6. Tumour growth delay study

Male BALB/c SCID mice were subcutaneously implanted in the left rear flank with HCT116 CRC cells. Once tumours reached a volume of 100 mm$^3$, mice were randomly allocated treatments of 1.5 mg/ kg of either $P_4$-SedU$_2$ only, 2:1 RALA/$P_4$-SedU$_2$ NPs or untreated. Treatments had no significant impact on the bodyweight of mice (Fig. 7 A). All Tumours developed visible dense vasculature after ~1 week of tumour size reaching 100 mm$^3$, indicating angiogenic factors were stimulated. This supports findings by Sun with ~1.4-fold increase of VEGF-A secretion in HCT116 in hypoxic conditions ($\leq$ 1% O$_2$) *in vitro* along with upregulation of CD31, CD34 and VE-cadherin [104] – endothelial factors that are associated with tumour vascular establishment [105–107]. Treatment regimens associated with 5-FU and associated adjuvants (*e.g* Leucorovin) [108,109] consist of single intravenous treatment weekly. Herein a single dose of 1.5 mg/kg$^{-1}$ $P_4$-SedU$_2$ was administered weekly for three weeks.

There is evidence of effective tumour growth inhibition during treatment with 2:1 RALA/$P_4$-SedU$_2$ NPs from day 0 to ~25 while the $P_4$-SedU$_2$ only group reveal no evidence of tumour growth inhibition compared to untreated control (Fig. 7 B). Throughout the course of the study, 2:1 RALA/$P_4$-SedU$_2$ NPs improved median survival from ~15 days to 29 days (Fig. 7 C) and significantly increased tumour doubling time from 9 days to 24 days (Fig. 7 D). The delay in tumour growth and improved survival of mice treated with RALA/$P_4$-SedU$_2$ NPs shows the utility of the RALA peptide used as a delivery vehicle to ensure intracellular delivery of the drug, resulting in a therapeutic effect. The free drug delivered without RALA was no more effective than control in delaying tumour growth or improving survival.

Tumour necrosis was apparent by the coring of the tumours and surrounding necrotic tissue when tumours approached 500 mm$^3$. Coring was only observed in the 2:1 RALA/$P_4$-SedU$_2$ NPs treatment group. Necrotic coring of a tumour is indicative of down regulation of angiogenic factors which constrains the vascularisation of the TME leading to perpetual hypoxia and glucose deprivation [110,111]. These findings correlate with other studies which have shown that selenols reduce MMP-2 and VEGF [49,87–89], contributing to down-regulation of angiogenesis causing tumour necrosis and destruction of neoplastic tissue [112–114].

Increased tumour growth was observed ~7 days after the final treatment, indicating that prolonged administration of this drug could retard this growth and could be possible as no rate-limiting toxicity was observed. It is possible that there is an upregulation of 'rescue' factors: Notch1, Cox-2, TGF-β, IL-8, FGF which would need to be measured.
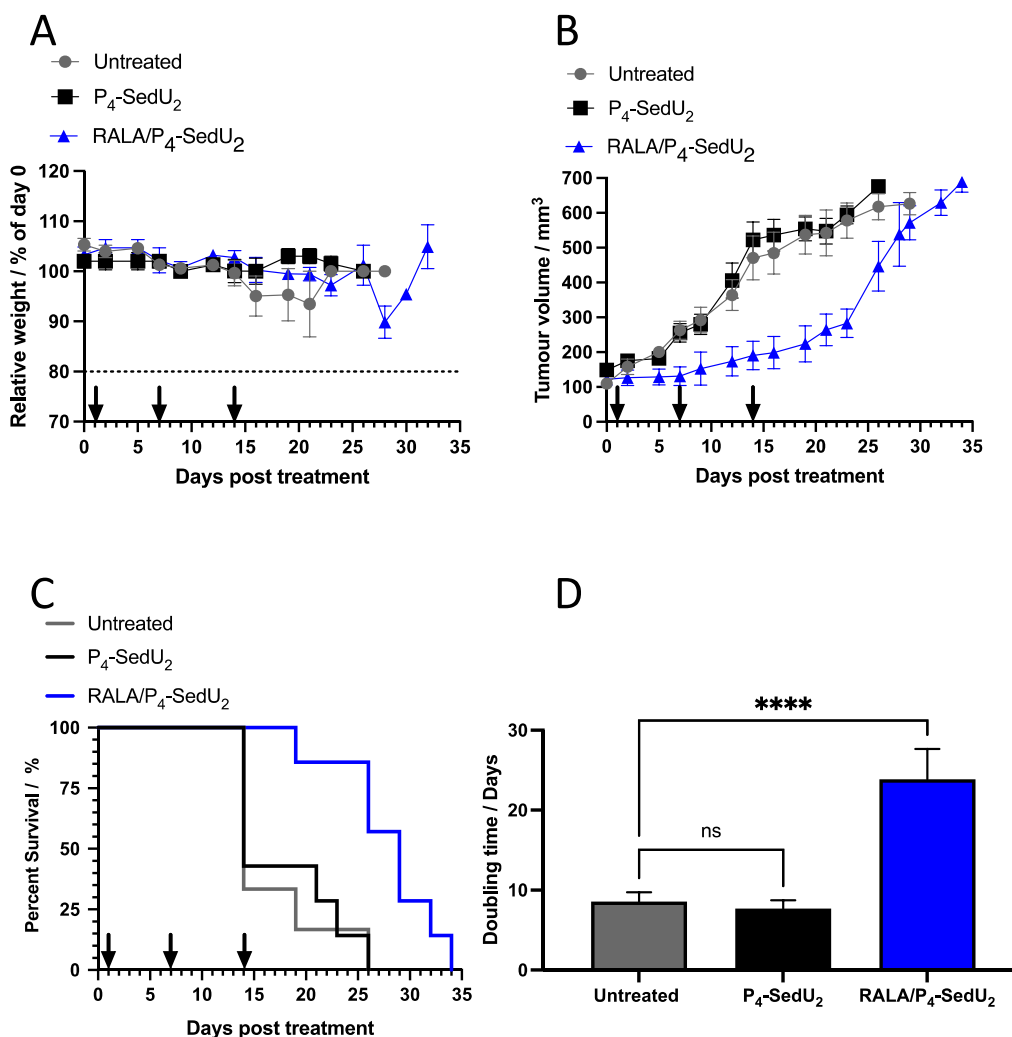
**Fig. 7.** Body mass, tumour growth and survival dynamics of treated BALB/c mice. A) Relative body mass of control and treated mice measured 3× per week. If body mass dropped ≥20% of starting mass, the mouse was culled. B) Tumour volume of control and treated mice over time with tumours measured 3× per week. C) Kaplan-Meier curve displaying percentage survival, with terminations occurring when tumours reached 650 mm$^3$. D) Tumour doubling time between day 0 and 14 (treatment 1 and 3). Arrows denote administration of treatments and $N = 6$.

Once the effects of 2:1 RALA/P$_4$-SedU$_2$ NPs wear off, the disproportionate presence of factors may cause elevated proliferation of the non-necrotic neoplastic tissue [115,116], putatively causing the observed sudden increase in tumour growth.

## 4. Conclusions

Synthesis of the dinucleoside tetraphosphates demonstrated effective swift coupling of short lived monophosphoroselenolate species with imidazolyl activated pyrophosphates to yield stable dinucleoside tetraphosphates. Using aqueous conditions to effect quick deprotection enables the divalent metal catalysis to accomplish rapid coupling that competes with the rate of spontaneous degradation of the monophosphoroselenolate. Moreover, this results in isolation of the material by RP-HPLC, desalting, and ion exchange. The synthesised compounds were stable in standard conditions (oxic, pH 7, room temperature). Further work on the synthesis should include varying reaction times, other divalent metal additives, and $^{77}$Se isotopic enrichment. Nucleotide modification research translates to other areas, including; anti-viral agents [16], mRNA cap analogues [117,118], systematic evolution of ligands by exponential enrichment (SELEX) [119] and mechanistic probes [120], indicating multiple biological and clinical applications.

## CRediT authorship contribution statement

**Jordan J. Wilson:** Writing – original draft, Methodology, Formal analysis, Data curation, Conceptualization. **Lindsey Bennie:** Writing – review & editing, Methodology, Investigation. **Olga Eguaogie:** Methodology, Investigation. **Ahmed Elkashif:** Writing – review & editing, Investigation. **Patrick F. Conlon:** Writing – review & editing, Validation. **Lynn Jena:** Methodology, Investigation. **Emma McErlean:** Investigation, Formal analysis. **Niamh Buckley:** Methodology, Formal analysis. **Klaudia Englert:** Methodology, Formal analysis. **Nicholas J. Dunne:** Supervision, Formal analysis. **James H.R. Tucker:** Supervision, Formal analysis. **Joseph S. Vyle:** Writing – review & editing, Writing – original draft, Supervision, Methodology, Funding acquisition, Formal analysis, Conceptualization. **Helen O. McCarthy:** Writing – review & editing, Supervision, Methodology, Funding acquisition, Formal analysis, Conceptualization.

## Data availability

Data will be made available on request.

## Appendix A. Supplementary data

The supporting information is available free of charge at www.lin khere.com

Supporting information contains extra details on the synthesis of the dinucleoside tetraphosphates, with full reaction conditions and methods including purification. NMR, HPLC and MS details, methods, and all corresponding spectra. Includes the formulation strategy and lyophilisation protocol for the RALA NPs. Primers used for RT-qPCR. All protocols used for *in vivo* experimentation to conduct all animal studies. Supplementary data to this article can be found online at https://doi. org/10.1016/j.jconrel.2024.03.036.

## References

[1] Cancer_Research_UK, Bowel Cancer Statistics. *https://www.cancerresearchuk. org/health-professional/cancer-statistics/statistics-by-cancer-type/bowel-cancer #heading-One*, 2021.

[2] N. Wasserberg, H.S. Kaufman, Palliation of colorectal cancer, Surg. Oncol. 16 (2007) 299–310.

[3] E. Dekker, P.J. Tanis, J.L.A. Vleugels, P.M. Kasi, M.B. Wallace, Colorectal cancer, Lancet 394 (2019) 1467–1480.

[4] D. Cunningham, et al., Colorectal cancer, Lancet 375 (2010) 1030–1047.

[5] A. Samanta, S. Dasgupta, T. Pathak, 5′-modified pyrimidine nucleosides as inhibitors of ribonuclease A, Bioorg. Med. Chem. 19 (2011) 2478–2484.

[6] G.L. Tritsch, Modified nucleosides with antineoplastic activity as inhibitors of an enzyme containing adenosine within its coenzyme, Cancer Res. 33 (1973) 310–312.

[7] C.M. Veenstra, J.C. Krauss, Emerging systemic therapies for colorectal cancer, Clin. Colon Rectal Surg. 31 (2018) 179–191.

[8] S. Blondy, et al., 5-fluorouracil resistance mechanisms in colorectal cancer: from classical pathways to promising processes, Cancer Sci. 111 (2020) 3142–3154.

[9] M.M. El-Hammadi, V. Delgado, C. Melguizo, J.C. Prados, J.L. Arias, Folic Acid-Decorated and PEGylated PLGA Nanoparticles for Improving the Antitumour Activity of 5-Fluorouracil, 2016, https://doi.org/10.1016/j. ijpharm.2016.11.012.

[10] C. Sethy, C.N. Kundu, 5-fluorouracil (5-FU) resistance and the new strategy to enhance the sensitivity against cancer: implication of DNA repair inhibition, Biomed. Pharmacother. 137 (2021).

[11] S. Azwar, H.F. Seow, M. Abdullah, M.F. Jabar, N. Mohtarrudin, Recent updates on mechanisms of resistance to 5-fluorouracil and reversal strategies in Colon Cancer treatment, Biology (Basel) 10 (2021).

[12] D.B. Longley, P.G. Johnston, Molecular mechanisms of drug resistance, J. Pathol. 205 (2005) 275–292.

[13] S.D. Webley, A. Hardcastle, R.D. Ladner, A.L. Jackman, G.W. Aherne, Deoxyuridine triphosphatase (dUTPase) expression and sensitivity to the thymidylate synthase (TS) inhibitor ZD9331, Br. J. Cancer 83 (2000) 792–799.

[14] S.D. Webley, S.J. Welsh, A.L. Jackman, G.W. Aherne, The ability to accumulate deoxyuridine triphosphate and cellular response to thymidylate synthase (TS) inhibition, Br. J. Cancer 85 (2001) 446–452.

[15] C.E. Canman, et al., Induction of resistance to Fluorodeoxyuridine cytotoxicity and DNA damage in human tumor cells by expression of Escherichia coli Deoxyuridinetriphosphatase, Cancer Res. 54 (1994) 2296–2298.

[16] S. Priet, J. Sire, G. Querat, Uracils as a cellular weapon against viruses and mechanisms of viral escape, Curr. HIV Res. 4 (2006) 31–42.

[17] C. Kerepesi, et al., Life without dUTPase, Front. Microbiol. 7 (2016) 1–10.

[18] C.E. Canman, H.-Y. Tang, D.P. Normollet, T.S. Lawrenceo, J. Maybaum, Variations in patterns of DNA damage induced in human colorectal tumor cells by 5-fluorodeoxyuridine: implications for mechanisms of resistance and cytotoxicity, Proc. Natl. Acad. Sci. 89 (1992) 10474–10478.

[19] P.M. Wilson, W. Fazzone, M.J. Labonte, H.J. Lenz, R.D. Ladner, Regulation of human dUTPase gene expression and p53-mediated transcriptional repression in response to oxaliplatin-induced DNA damage, Nucleic Acids Res. 37 (2009) 78–95.

[20] H. Hernández-Vargas, et al., Transcriptional profiling of MCF7 breast cancer cells in response to 5-flouracil: relationship with cell cycle changes and apoptosis, and identification of novel targets of p53, Int. J. Cancer 119 (2006) 1164–1175.

[21] S.C. Lee, J. Chan, M.V. Clement, S. Pervaiz, Functional proteomics of resveratrol-induced colon cancer cell apoptosis: Caspase-6-mediated cleavage of Lamin A is a major signaling loop, Proteomics 6 (2006) 2386–2394.

[22] K.M. Kim, et al., Clinical significance of p53 protein expression and TP53 variation status in colorectal cancer, BMC Cancer 22 (2022) 1–17.

[23] D. Ji, A.M. Kietrys, Y. Lee, E.T. Kool, ATP-linked chimeric nucleotide as a specific luminescence reporter of Deoxyuridine Triphosphatase, Bioconjug. Chem. 29 (2018) 1614–1621.

[24] C.E. Canman, T.S. Lawrence, D.S. Shewach, H.Y. Tang, J. Maybaum, Resistance to Fluorodeoxyuridine-induced DNA damage and cytotoxicity correlates with an elevation of Deoxyuridine Triphosphatase activity and failure to accumulate Deoxyuridine triphosphate, Cancer Res. 53 (1993) 5219–5224.

[25] J. Zhang, et al., The role of nucleoside transporters in cancer chemotherapy with nucleoside drugs, Cancer Metastasis Rev. 26 (2007) 85–110.

[26] M. Michel, L. Kaps, A. Maderer, P.R. Galle, M. Moehler, The role of p53 dysfunction in colorectal cancer and its implication for therapy, Cancers (Basel) 13 (2021) 1–24.

[27] H.E. Krokan, F. Drabløs, G. Slupphaug, Uracil in DNA – occurrence, consequences and repair, Oncogene 21 (2002) 8935–8948.

[28] Y. Liu, et al., Coordination of steps in Single-Nucleotide Base excision repair mediated by Apurinic / Apyrimidinic endonuclease 1 and DNA polymerase, J. Biol. Chem. 282 (2007) 13532–13541.

[29] T. Lindahl, Suppression of spontaneous mutagenesis in human cells by DNA base excision-repair, Mutat. Res. Rev. Mutat. Res. 462 (2000) 129–135.

[30] V. Bailly, M. Derydt, W.G. Verly, 5-elimination in the repair of AP (apurinic / apyrimidinic) sites in DNA, Biochem. J. 261 (1989) 707–713.

[31] J.B. Rodriguez, C. Gallo-Rodriguez, The role of the phosphorus atom in drug design, ChemMedChem 14 (2019) 190–216.

[32] D. Mevorach, Opsonization of apoptotic cells: implications for uptake and autoimmunity, Ann. N. Y. Acad. Sci. 926 (2000) 226–235.

[33] J.I. Fletcher, M. Haber, M.J. Henderson, M.D. Norris, ABC transporters in cancer : more than just drug efflux pumps, Nat. Rev. Cancer 10 (2010) 143–156.

[34] H. Zimmermann, M. Zebisch, N. Sträter, Cellular function and molecular structure of ecto-nucleotidases, Purinergic Signal 8 (2012) 437–502.

[35] E.M. McErlean, C.M. McCrudden, H.O. McCarthy, Multifunctional delivery Systems for Cancer Gene Therapy, Gene Ther. Princip. Challenges 91 (2015) 57–104.

[36] M. Emma, M. Cian, O. Helen, Delivery of nucleic acids for cancer gene therapy: overcoming extra- and intra- cellular barriers, Ther. Deliv. 5 (2014) 1297–1314.

[37] A.S. Massey, et al., Potentiating the anticancer properties of bisphosphonates by Nanocomplexation with the cationic amphipathic peptide, RALA, Mol. Pharm. 13 (2016) 1217–1228.

[38] H.O. Mccarthy, et al., Development and characterization of self-assembling nanoparticles using a bio-inspired amphipathic peptide for gene delivery, J. Control. Release 189 (2014) 141–149.

[39] Y. Liu, et al., Development and characterization of high efficacy cell-penetrating peptide via modulation of the histidine and arginine ratio for gene therapy, Materials 14 (2021) 4674.

[40] J. McCaffrey, et al., Transcending epithelial and intracellular biological barriers; A prototype DNA delivery device, J. Control. Release 226 (2016) 238–247.

[41] M. Zimisa, J.J. Wilson, McErlean Emma, Dunne Nicholas, H.O. Mccarthy, Synthesis and evaluation of a Thermoresponsive degradable chitosan-grafted PNIPAAm hydrogel as a "Smart" gene delivery system Monika, Materials 13 (2020) 2530–2552.

[42] E.J. Mulholland, N. Dunne, H.O. McCarthy, MicroRNA as therapeutic targets for chronic wound healing, Mol. Ther. Nucleic Acids 8 (2017) 46–55.

[43] J.M. Sadowska, et al., Development of miR-26a-activated scaffold to promote healing of critical-sized bone defects through angiogenic and osteogenic mechanisms, Biomaterials 303 (2023) 122398.

[44] J. McCaffrey, et al., Transcending epithelial and intracellular biological barriers; a prototype DNA delivery device, J. Control. Release 226 (2016) 238–247.

[45] L.A. Bennie, H.O. McCarthy, J.A. Coulter, Enhanced nanoparticle delivery exploiting tumour-responsive formulations, Cancer Nanotechnol. 9 (2018) 1–20.

[46] J.R. Casey, S. Grinstein, J. Orlowski, Sensors and regulators of intracellular pH, Nat. Rev. Mol. Cell Biol. 11 (2009) 50–61.

[47] Y.B. Hu, E.B. Dammer, R.J. Ren, G. Wang, The endosomal-lysosomal system: from acidification and cargo sorting to neurodegeneration, Transl. Neurodegener. 4 (2015) 1–10.

[48] M. Álvarez-Pérez, W. Ali, M.A. Marć, J. Handzlik, E. Domínguez-Álvarez, Selenides and diselenides: A review of their anticancer and chemopreventive activity, Molecules 23 (2018) 1–19.

[49] J. Lu, C. Jiang, Antiangiogenic activity of selenium in cancer chemoprevention: metabolite-specific effects, Nutr. Cancer 40 (2001) 64–73.

[50] A. Razaghi, M. Poorebrahim, D. Sarhan, M. Björnstedt, Selenium stimulates the antitumour immunity: insights to future research, Eur. J. Cancer 155 (2021) 256–267.

[51] P.F. Conlon, et al., Solid-phase synthesis and structural characterisation of phosphoroselenolate-modified DNA: a backbone analogue which does not impose conformational bias and facilitates SAD X-ray crystallography, Chem. Sci. 10 (2019) 10948–10957.

[52] K. Nyíri, et al., Structural model of human dUTPase in complex with a novel proteinaceous inhibitor, Sci. Rep. 8 (2018) 1–15.

[53] M.P. Rayman, Selenium in cancer prevention: a review of the evidence and mechanism of action, Proc. Nutr. Soc. 64 (2005) 527–542.

[54] N.A.P. Franken, H.M. Rodermond, J. Stap, J. Haveman, C. van Bree, Clonogenic assay of cells in vitro, Nat. Protoc. 1 (2006) 2315–2319.

[55] S. Warnecke, C. Meier, Synthesis of nucleoside di- and triphosphates and dinucleoside polyphosphates with cyclosal-nucleotides, J. Organomet. Chem. 74 (2009) 3024–3030.

[56] B. Borecka, J. Chonjnowski, M. Cypryk, J. Michalski, J. Zielinska, Synthetic and mechanistic aspects of the reaction of trialkylsilyl halides with thio and seleno esters of phosphorous, J. Organomet. Chem. 171 (1979) 17–34.

[57] S. Mikkola, et al., 5′-Chalcogen-substituted nucleoside pyrophosphate and phosphate monoester analogues: preparation and hydrolysis studies, Int. J. Mol. Sci. 23 (2022).

[58] O. Eguaogie, J.S. Vyle, Vibration Ball Milling for the Synthesis of 5 -Thioadenosine 5 -Pyrophosphate (P → 5) Adenosine (dASppA), Curr. Protoc. Nucleic Acid Chem. 70 (2017) 1–12.

[59] O. Eguaogie, et al., Synthesis of novel pyrophosphorothiolate-linked dinucleoside cap analogues in a ball mill, Org. Biomol. Chem. 14 (2016) 1201–1205.

[60] L. Appy, et al., Straightforward ball-milling access to Dinucleoside 5′,5′-polyphosphates through Phosphorimidazolide intermediates, Chem. Eur. J. 25 (2019) 2477–2481.

[61] L. Appy, C. Chardet, S. Peyrottes, Synthetic Strategies for Dinucleotides Synthesis, 2019.

[62] I.B. Yanachkov, E.J. Dix, M.I. Yanachkova, G.E. Wright, P1 and P2-Diimidazolyl derivatives of pyrophosphate and bis-phosphonates. Synthesis, properties and use in preparation of dinucleotide tetraphosphates and analogs, Org. Biomol. Chem. 9 (2011) 730–738.

[63] L. Wu, J. Zhang, W. Watanabe, Physical and chemical stability of drug nanoparticles, Adv. Drug Deliv. Rev. 63 (2011) 456–469.

[64] A.S. Massey, et al., Potentiating the anticancer properties of bisphosphonates by Nanocomplexation with the cationic amphipathic peptide, RALA, Mol. Pharm. 13 (2016) 1217–1228.

[65] W. Jiang, B.Y.S. Kim, J.T. Rutka, W.C.W. Chan, Nanoparticle-mediated cellular response is size-dependent, Nat. Nanotechnol. 3 (2008) 145–150.

[66] X.A. Li, W.V. Everson, E.J. Smart, Caveolae, lipid rafts, and vascular disease, Trends Cardiovasc. Med. 15 (2005) 92–96.

[67] Pawan Kumar, Michael E. Østergaard, Bharat Baral, Brooke A. Anderson, Dale C. Guenther, Mamta Kaura, Daniel J. Raible, Synthesis and biophysical properties of C5-functionalized LNA, Methods Mol. Biol. 535 (2009) 165–186.

[68] S.E. Koehler, R.D. Ladner, Small interfering RNA-mediated suppression of dUTPase sensitizes cancer cell lines to thymidylate synthase inhibition, Mol. Pharmacol. 66 (2004) 620–626.

[69] M.D. Kaeser, S. Pebernard, R.D. Iggo, Regulation of p53 stability and function in HCT116 Colon Cancer cells, J. Biol. Chem. 279 (2004) 7598–7605.

[70] A. Rajput, et al., Characterization of HCT116 human Colon Cancer cells in an Orthotopic model, J. Surg. Res. 147 (2008) 276–281.

[71] F.M. Menzies, A. Fleming, D.C. Rubinsztein, Compromised autophagy and neurodegenerative diseases, Nat. Publ. Group 16 (2015).

[72] J. Sharma, A. Ronza, P. Lotfi, M. Sardiello, Lysosomes and brain health, Annu. Rev. Neurosci. 41 (2018) 255–276.

[73] N. Cheng, S. Chen, J. Li, T. Young, Short-term spheroid formation enhances the regenerative capacity of adipose-derived stem cells by promoting stemness, angiogenesis, and chemotaxis, Stem Cells Transl. Med. 2 (2013) 584–594.

[74] Q. Zhang, et al., Three-dimensional spheroid culture of human gingiva-derived mesenchymal stem cells enhances mitigation of chemotherapy-induced Oral mucositis, Stem Cells Dev. 21 (2012) 937–947.

[75] A. Tchoryk, et al., Penetration and uptake of nanoparticles in 3D tumor spheroids, Bioconjug. Chem. 30 (2019) 1371–1384.

[76] I. Van Zundert, B. Fortuni, S. Rocha, From 2d to 3d cancer cell models—the enigmas of drug delivery research, Nanomaterials 10 (2020) 1–30.

[77] A. O`keeffe, et al., Novel 2D and 3D assays to determine the activity of anti-leishmanial drugs, Microorganisms 8 (2020) 1–22.

[78] L.A. Wessjohann, A. Schneider, M. Abbas, W. Brandt, Selenium in chemistry and biochemistry in comparison to sulfur, Biol. Chem. 388 (2007) 997–1006.

[79] S. Si, P. Saftig, J. Klumperman, Lysosome biogenesis and lysosomal membrane proteins : trafficking meets function, Nat. Rev. Mol. Cell Biol. 10 (2009) 623–635.

[80] N. Tiwari, et al., The SrrAB two-component system regulates Staphylococcus aureus pathogenicity through redox sensitive cysteines, Proc. Natl. Acad. Sci. 117 (2020) 10989–10999.

[81] H. Kuivaniemi, et al., in: H. Kuivaniemi, G. Tromp (Eds.), Type III collagen (COL3A1): Gene and protein structure, tissue distribution and associated diseases vol. 707, 2020, pp. 151–171.

[82] A.L. Samson, et al., Nucleocytoplasmic coagulation: an injury-induced aggregation event that disulfide crosslinks proteins and facilitates their removal by plasmin, Cell Rep. 2 (2012) 889–901.

[83] D. Anton, H. Burckel, E. Josset, G. Noel, Three-dimensional cell culture: A breakthrough in vivo, Int. J. Mol. Sci. 16 (2015) 5517–5527.

[84] S. Thippabhotla, C. Zhong, M. He, 3D cell culture stimulates the secretion of in vivo like extracellular vesicles, Sci. Rep. 9 (2019) 1–14.

[85] R. Edmondson, J.J. Broglie, A.F. Adcock, L. Yang, Three-dimensional cell culture systems and their applications in drug discovery and cell-based biosensors, Assay Drug Dev. Technol. 12 (2014) 207–218.

[86] J.E. Szabó, E. Takács, G. Merényi, B.G. Vértessy, J. Tóth, Trading in cooperativity for specificity to maintain uracil-free, Nat. Publ. Group 1–12 (2016), https://doi.org/10.1038/srep24219.

[87] J. Pinto, J. Lee, R. Sinha, A. Cooper, Chemopreventive mechanisms of α-keto acid metabolites of naturally occurring organoselenium compounds, Amino Acids 41 (2011) 29–41.

[88] H. Zeng, M. Wu, J.H. Botnen, Methylselenol, a selenium metabolite, induces cell cycle arrest in G1 phase and apoptosis via the extracellular-regulated kinase 1/2 pathway and other cancer signaling genes, J. Nutr. 139 (2009) 1613–1618.

[89] H. Zeng, M. Briske-Anderson, M. Wu, M.P. Moyer, Methylselenol, a selenium metabolite, plays common and different roles in cancerous colon HCT116 cell and noncancerous NCM460 colon cell proliferation, Nutr. Cancer 64 (2012) 128–135.

[90] R. Kirchies, et al., Coupling of cell-binding ligands to polyethylenimine for targeted gene delivery, Gene Ther. 4 (1997) 409–418.

[91] R. Zhang, X. Qin, F. Kong, P. Chen, G. Pan, Improving cellular uptake of therapeutic entities through interaction with components of cell membrane, Drug Deliv. 26 (2019) 328–342.

[92] D.E. Owens, N.A. Peppas, Opsonization, biodistribution, and pharmacokinetics of polymeric nanoparticles, Int. J. Pharm. 307 (2006) 93–102.

[93] A.E. Green, P.G. Rose, Pegylated liposomal doxorubicin in ovarian cancer, Int. J. Nanomedicine 1 (2006) 229–239.

[94] J. Delahousse, C. Skarbek, A. Paci, Prodrugs as drug delivery system in oncology, Cancer Chemother. Pharmacol. 84 (2019) 937–958.

[95] M. Markovic, S. Ben-shabat, Prodrugs for improved drug delivery : lessons learned from recently developed and marketed products, Pharmaceutics 12 (2020) 1031–1043.

[96] M. Morachis, E.A. Mahmoud, A. Almutairi, Physical and chemical strategies for therapeutic delivery by using polymeric nanoparticles, Pharmacol. Rev. 64 (2012) 505–519.

[97] INTERNATIONAL STANDARD ISO 10993-5, ISO vols. 10993-5:2009(E) 1–40, 2009.

[98] I. Midgley, et al., Pharmacokinetics and metabolism of the prodrug DB289 (2,5-Bis[4-(N-methoxyamidino)phenyl]furan Monomaleate) in rat and monkey and its conversion to the antiprotozoal/antifungal drug DB75 (2,5-Bis(4-guanylphenyl) furan Dihydrochloride), Pharmacology 35 (2007) 955–967.

[99] N. Mehrotra, M. Gupta, A. Kovar, B. Meibohm, The role of pharmacokinetics and pharmacodynamics in phosphodiesterase-5 inhibitor therapy, Int. J. Impot. Res. 19 (2007) 253–264.

[100] S. Cho, Y.R. Yoon, Understanding the pharmacokinetics of prodrug and metabolite, Transl. Clin. Pharmacol. 26 (2018) 1–5.

[101] V. Khare, et al., Long-circulatory nanoparticles for gemcitabine delivery: development and investigation of pharmacokinetics and in-vivo anticancer efficacy, Eur. J. Pharm. Sci. 92 (2016) 183–193.

[102] M.H. Haugen, K. Flatmark, S.O. Mikalsen, G.M. Malandsmo, The metastasis-associated protein S100A4 exists in several charged variants suggesting the presence of posttranslational modifications, BMC Cancer 8 (2008).

[103] K.J. Chen, A.J. Plaunt, F.G. Leifer, J.Y. Kang, D. Cipolla, Recent advances in prodrug-based nanoparticle therapeutics, Eur. J. Pharm. Biopharm. 165 (2021) 219–243.

[104] Z. Liu, L. Qi, Y. Li, X. Zhao, B. Sun, VEGFR2 regulates endothelial differentiation of colon cancer cells, BMC Cancer 17 (2017) 1–11.

[105] P. Carmeliet, et al., Targeted deficiency or cytosolic truncation of the VE-cadherin gene in mice impairs VEGF-mediated endothelial survival and angiogenesis, Cell 98 (1999) 147–157.

[106] D.G. Tang, et al., Identification of PECAM-1 in solid tumor cells and its potential involvement in tumor cell adhesion to endothelium, J. Biol. Chem. 268 (1993) 22883–22894.

[107] J.S. Nielsen, K.M. McNagny, Novel functions of the CD34 family, J. Cell Sci. 121 (2008) 4145.

[108] W. Schippinger, et al., A prospective randomised phase III trial of adjuvant chemotherapy with 5-fluorouracil and leucovorin in patients with stage II colon cancer, Br. J. Cancer 97 (2007) 1021–1027.

[109] N. Petrelli, et al., The modulation of fluorouracil with leucovorin in metastatic colorectal carcinoma: A prospective randomized phase III trial, J. Clin. Oncol. 7 (1989) 1419–1426.

[110] D. Jiao, et al., Necroptosis of tumor cells leads to tumor necrosis and promotes tumor metastasis, Cell Res. 28 (2018) 868–870.

[111] S. Cui, Formation of necrotic cores in the growth of tumor: analytic results, Acta Math. Sci. 26 (2006) 781–796.

[112] O.R.F. Mook, W.M. Frederiks, C.J.F. Van Noorden, The role of gelatinases in colorectal cancer progression and metastasis, Biochim. Biophys. Acta Rev. Cancer 1705 (2004) 69–89.

[113] L.G. Presta, et al., Humanization of an anti-vascular endothelial growth factor monoclonal antibody for the therapy of solid tumors and other disorders, Cancer Res. 57 (1997) 4593–4599.

[114] K. Holmes, O.L. Roberts, A.M. Thomas, M.J. Cross, Vascular endothelial growth factor receptor-2: structure, function, intracellular signalling and therapeutic inhibition, Cell. Signal. 19 (2007) 2003–2012.

[115] M. Potente, H. Gerhardt, P. Carmeliet, Review basic and therapeutic aspects of angiogenesis, Cell 146 (2011) 873–887.

[116] Z.G. Liu, D. Jiao, Necroptosis, tumor necrosis and tumorigenesis, Cell Stress 4 (2020) 1–8.

[117] M. Ziemniak, et al., Phosphate-modified analogues of m7GTP and m7Gppppm7G - Synthesis and biochemical properties, Bioorg. Med. Chem. 23 (2015) 5369–5381.

[118] B.A. Wojtczak, et al., 5′-Phosphorothiolate dinucleotide cap analogues: reagents for messenger RNA modification and potent small-molecular inhibitors of Decapping enzymes, J. Am. Chem. Soc. 140 (2018) 5987–5999.

[119] L. Gold, SELEX: how it happened and where it will go, J. Mol. Evol. 81 (2015) 140–143.

[120] F. Sanger, S. Nicklen, A.R. Coulson, DNA sequencing with chain-terminating inhibitors, Proc. Natl. Acad. Sci. 74 (1977) 5463–5467.